Uncertainty quantification for stellar population-kinematics models of galaxies

Progress report

Fabian Parzer

May 6, 2021

1 Short overview

- The reconstruction algorithms both with and without curvelets are implemented. The results without curvelets are okay, but the results with curvelets are disappointing.
- Even at a signal-to-noise ratio of 2000, bad reconstructions are still consistent with the noisy measurement (in the sense that they have the same data misfit as the true parameter value).
- Two algorithms for uncertainty quantification were implemented: The first is based on a nonlinear reparametrization combined with a Gaussian approximation. The second is based on a concentration inequality combined with convex optimization. They compute what might be called "projected credible intervals".
  - *(i)* The first approach for uncertainty quantification works for the pixel-based approach, but runs into numerical difficulties for the curvelet-based approach.
  - *(ii)* The second approach is extremely slow and currently doesn't really work.

2 Reconstruction methods

2.1 Pixel-based reconstruction

Currently, for the pixel-based reconstruction we solve the optimization problem

$$\begin{aligned} \min_{f,\theta_v} \quad & \{\frac{1}{\delta^2}\left\|\hat{y}-\mathcal{G}(f,\theta_v)\right\|_2^2+\beta_f\left\|\Sigma_f^{-1/2}(f-\bar{f})\right\|+\beta_{\theta_v}\left\|\Sigma_{\theta_v}^{-1/2}(\theta_v-\bar{\theta}_v)\right\|_2^2\}, \\ \text{subject to} \quad & f\geq 0, \end{aligned} \tag{2.1}$$

where

- $\hat{y}=y+\delta\xi$ is the noisy measurement. Here, $\xi\sim\mathcal{N}(0,\mathbb{I})$ is a standard normal distributed random vector and $\delta>0$ is the noise standard deviation.
- $\bar{f}$ and $\bar{\theta}_v$ are the prior means for f and θ_v. Currently, we use $\bar{f}=0$.
- Σ_f and Σ_{θ_v} are the covariance matrices. Currently, we are using the values $\Sigma_f=\mathbb{I}$, $\Sigma_{\theta_v}=\text{diag}(10,10,1,1,1,1,1)$, where $\mathbb{I}$ denotes the identity matrix.
- $\beta_f>0$ and $\beta_{\theta_v}>0$ are the regularization parameters. Their values were determined by trial and error.

We tested the reconstruction algorithm with a signal-to-noise ratio of 2000, where the signal-to-noise ratio is defined as

$$\mathrm{SNR}(\hat{y}) := \frac{\|y\|_2}{\|\hat{y} - y\|_2}.$$

The "true" distribution function f^* was generated using Prashin's random Gaussian mixture generator, while θ_v^* was always set to $\theta_v^* = [30, 100, 1, 0, 0, -0.05, 0.1]$.

The results are visualized in figures Figure 2 and **??**.

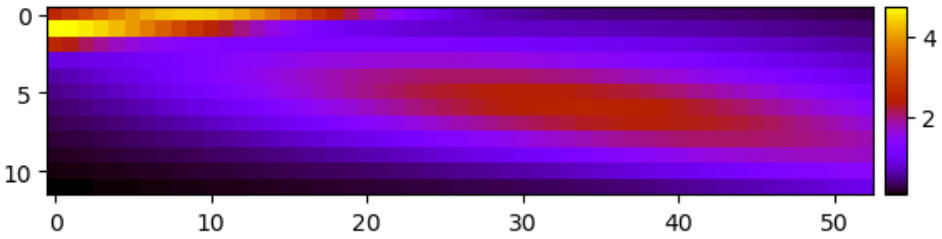

(A) *The true distribution function.*

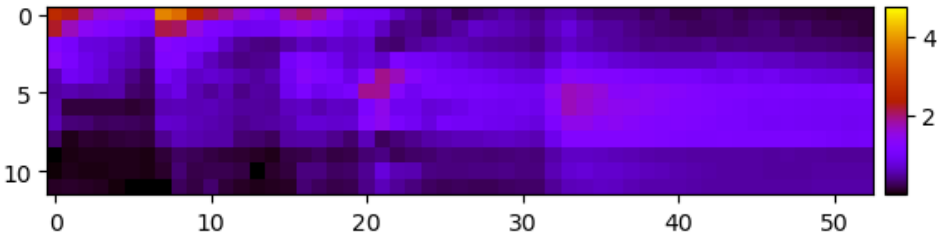

(B) *The MAP estimate.*

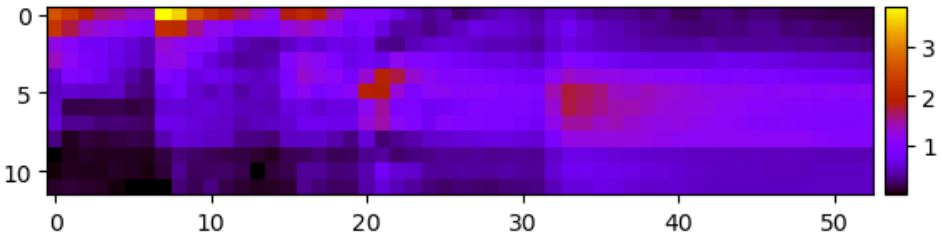

(C) *The MAP estimate rescaled.*

FIGURE 1. *The results for a signal-to-noise ratio of 2000. One sees that the MAP estimate recovers the rough structure of the distribution function. However, it does not seem to recover the mass, as it is much smaller. This can be seen by scaling up the MAP estimate, which is then visually much closer to the ground truth.*

We observe:

- The MAP estimate captures the rough shape of the original distribution function, but it does not capture the overall mass, as lives on a much smaller scale.
- Nevertheless, the MAP estimate is consistent with the data. If we denote with $y_{\mathrm{MAP}} = \mathcal{G}(x_{\mathrm{MAP}})$ the predicted data according to the MAP estimate, one can actually see that

  $$\frac{\|y_{\mathrm{MAP}} - y\|}{\|\hat{y} - y\|} \approx 1,$$

  i.e. the misfit of the MAP estimate is almost the same as the size of the noise. This means we can probably only improve the reconstruction by using different regularization that takes advantage of further prior knowledge. For example, we could use a suitable differential operator in the regularization term for the distribution function f.
- We also observed in the numerical experiments that unless the starting value for θ_v is close to the true value, the optimization takes very long.

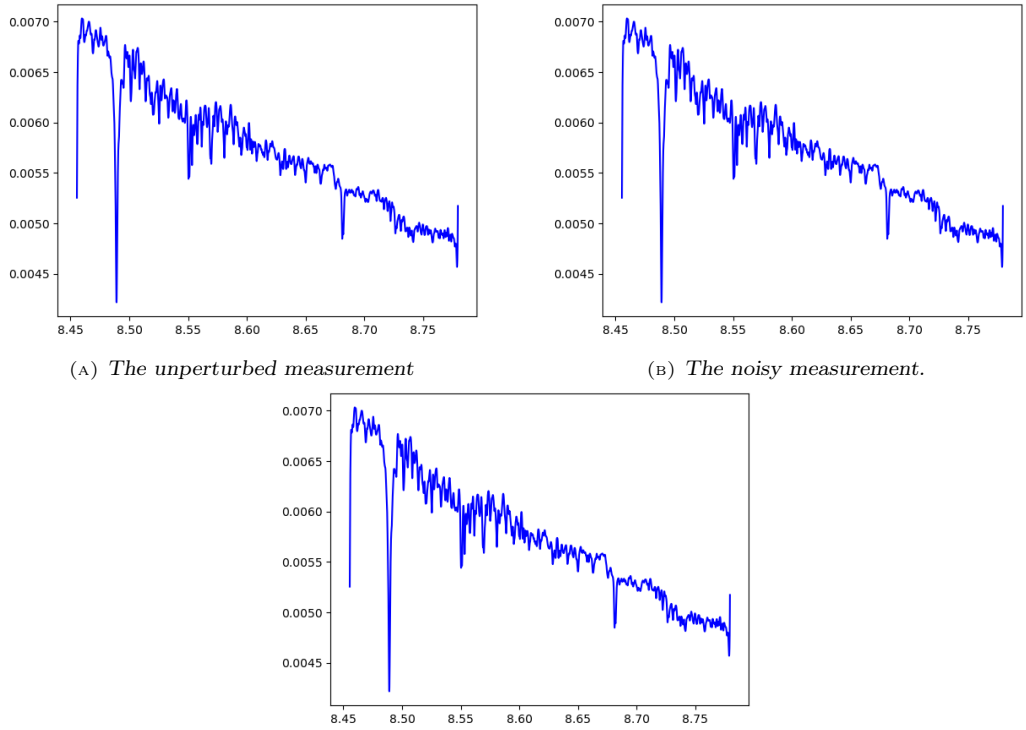

(A) *The unperturbed measurement*

(B) *The noisy measurement.*

(C) *The predicted measurement* y_{MAP}.

FIGURE 2. *The noisy measurement and the predicted measurement* $y_{\mathrm{MAP}} = \mathcal{G}(x_{\mathrm{MAP}})$ *of the MAP estimate. They are virtually indistinguishable, even though the MAP estimate is rather poor.*

2.2 Curvelet-based reconstruction

For the curvelet-based reconstruction, we solve almost the same optimization problem

$$\begin{aligned} \min_{f,\theta_v} \quad & \{\frac{1}{\delta^2}\left\|\hat{y} - \mathcal{G}(f,\theta_v)\right\|_2^2 + \beta_f \left\|\Phi f\right\|_1 + \beta_{\theta_v} \left\|\Sigma_{\theta_v}^{-1/2}(\theta_v - \bar{\theta}_v\right\|_2^2\}, \\ \text{subject to} \quad & f \geq 0. \end{aligned} \tag{2.2}$$

The only change is in the regularization term for f. Here, $\Phi : \mathbb{R}^{n_f} \to \mathbb{R}^N$ is the curvelet frame operator that maps an image to its N curvelets coefficients (with $N \gg n_f$).

With the same signal-to-noise ratio and the same ground truth f_*, the curvelet-based reconstructions are visualized in figures Figure 3 and Figure 4

During the numerical experiments, we observed the following:

- The transformation-based optimization method seems to be not ideal, as it transforms the simple nonnegativity constraint into a computationally much more cumbersome nonlinear constraint. Maybe it will be worth the time to implement a different approach.
- The curvelet-based approach is computationally much more expensive, as it increases the dimension of the optimization problem by a factor of almost 10.
- At the same time, the curvelet-based reconstruction tends to be concentrated at distinct round blobs, which is probably undesirable for our purposes.

3 Mode-based uncertainty quantification

Next, we discuss our mode-based approach to uncertainty quantification. The advantage of this approach is that it does not integrate the complete statistical model, which would be costly and difficult, but

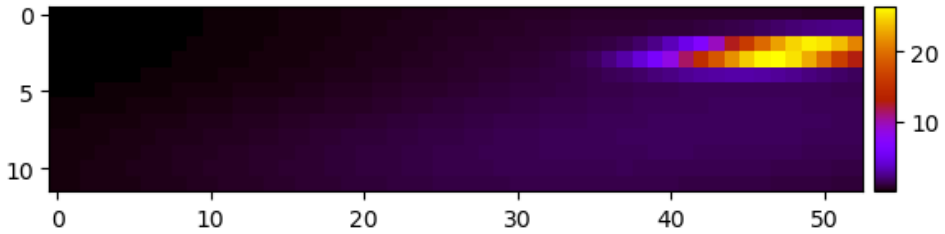

(A) *The true distribution function.*

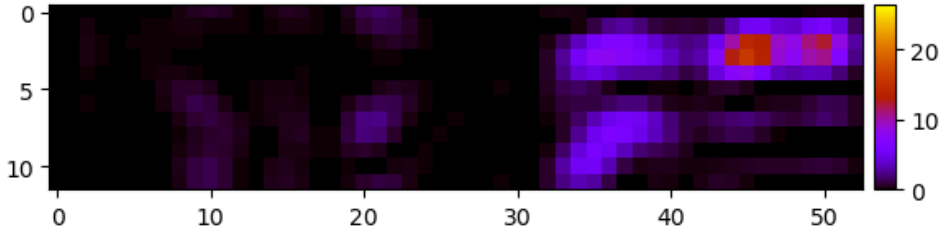

(B) *The reconstruction (with curvelets).*

FIGURE 3. *The reconstruction using curvelets. The curvelet basis causes the reconstruction to be concentrated at distinct round "blobs", and creates artifacts.*

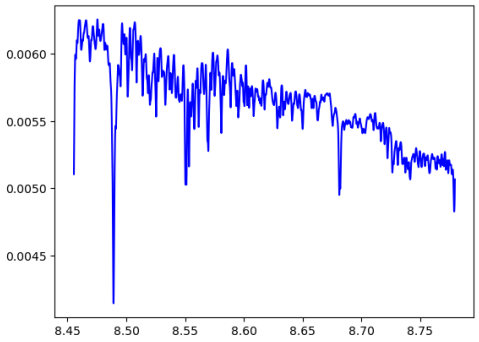

(A) *The unperturbed measurement*

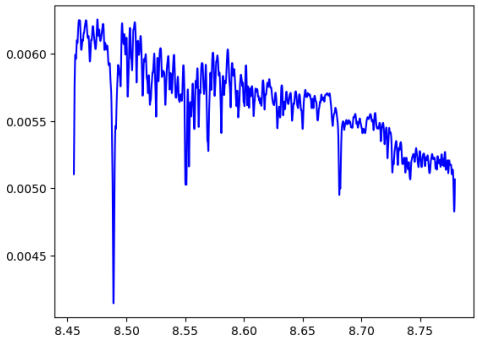

(B) *The noisy measurement.*

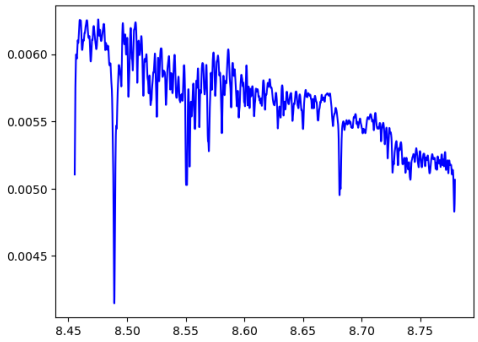

(C) *The predicted measurement* y_{MAP}.

FIGURE 4. *The noisy measurement compared with the measurement corresponding to the curvelet reconstruction. Again, the normalized misfit of the reconstruction is very close to 1, which means that the estimate is consistent with the data. The fact that this happens at a signal-to-noise ratio of 2000 is noteworthy.*

provides inference based on an approximation of the posterior distribution around its mode, the maximum-a-posteriori estimate, which is computed by solving the optimization problem from Section 2. We tested two methods that compute (approximations of) projected credible intervals, which provide for each pixel an interval in which the pixel is expected to lie with a given probability.

3.1 Credible regions

For highdimensional parameters, the covariance matrix might not be the best tool for inference, since it will be a large matrix that you cannot just "look at". A more intuitive tool are confidence regions, whose Bayesian counterpars are called credible or — more precisely — highest-probability-density regions (HPD regions).

Definition 3.1 (Credible region) Let $p(x)$ be a probability density function on $\mathbb{R}^n$ and $\alpha \in (0,1)$. Then, we call a set $C_\alpha(x) \subset \mathbb{R}^n$ a $(1-\alpha)$-credible region of $p(x)$ if

$$C_\alpha(x) \in \operatorname*{argmin}_{S \subset \mathbb{R}^n} \left\{ \operatorname{vol}(S) : \int_S p(x)\,\mathrm{d}x \geq 1-\alpha \right\}. \tag{3.1}$$

Note that credible regions are seldom unique, since one can add and subtract arbitrary sets of probability zero without affecting (3.1). For our purposes, this problem is however irrelevant.

In imaging, a credible region is a subset of the high-dimensional parameter space. Consequently, it is cumbersome to work directly with credible regions, as they are impossible to visualize for more than three dimensions. One can compute however various quantities from these credible regions that are easier to visualize. We will now present 3 different ways to visualize a given credible region $C_\alpha(x)$. Then, in the next section we will consider two ways of actually obtaining approximate credible regions in a way that can be used for actual computations.

Minimally/maximally regularized elements

Given a credible region $C_\alpha(x) \subset \mathbb{R}^n$, one can always compute the maximizer and minimizer of a given regularization term in this region. For problem (2.1), this would mean that given a credible region $C_\alpha(f, \theta_v)$, we would compute

$$(f_{\text{maxreg}}, \theta_{v,\text{maxreg}}) \in \operatorname{argmin} \left\{ \beta_f \left\| \Sigma_f^{-1/2}(f - \bar{f}) \right\|_2^2 + \beta_{\theta_v} \left\| \Sigma_{\theta_v}^{-1/2}(\theta_v - \bar{\theta}_v) \right\|_2^2 : f, \theta_v \in C_\alpha(f, \theta_v) \right\},$$
$$(f_{\text{minreg}}, \theta_{v,\text{minreg}}) \in \operatorname{argmin} \left\{ \beta_f \left\| \Sigma_f^{-1/2}(f - \bar{f}) \right\|_2^2 + \beta_{\theta_v} \left\| \Sigma_{\theta_v}^{-1/2}(\theta_v - \bar{\theta}_v) \right\|_2^2 : f, \theta_v \in C_\alpha(f, \theta_v) \right\}.$$

The element $(f_{\text{maxreg}}, \theta_{v,\text{maxreg}})$ can then be interpreted as the smallest (because it *minimizes* the regularization term and is thus *maximally regularized*) element in the credible region $C_\alpha(f, \theta_v)$. Correspondingly, the element $(f_{\text{maxreg}}, \theta_{v,\text{maxreg}})$ is the largest (in the sense that it is minimally regularized, as it *maximizes* the regularization term) element in the credible region.

The maximally and minimally regularized elements can then be easily visualized. By looking at them, one can get a feeling for how much variation around the MAP estimate is possible in the high-dimensional posterior credible region.

However, there is a major caveat: The maximally and minimally regularized credible elements cannot be interpreted as giving a range between the "credible values" of the parameters f and θ_v lie. If we fix a pixel, there might in general exist many elements in the credible region $C_\alpha(f, \theta_v)$ that take smaller or smaller larger values than the maximally and minimally regularized element on that given pixel.

However, the minimally and maximally regularized credible elements are in general the cheapest visualizations to compute, as one only has to solve two optimization problems.

Locally credible intervals

In [1], the authors proposed so-called "local credible intervals", which provide some kind of "error bars" around the MAP estimate. As we will see below, this interpretation has to be taken with a grain of salt.

In the following, we let

$$[n] := \{1, \dots, n\} \subset \mathbb{N},$$

and $\mathfrak{P}(S)$ denote the power set of a given set S.

Then, local credible intervals are formally defined as follows.

Definition 3.2 (Local credible interval) Let $C_\alpha(x)$ be a posterior credible region and $\hat{x}$ be a MAP estimate. Let furthermore $\mathcal{I} = \{I_1, \dots, I_J\} \subset \mathfrak{P}([n])$ be a partition of $[n]$. Let the vectors $\zeta_1, \dots, \zeta_J \in \mathbb{R}^n$ be given by

$$(\zeta_j)_i = \begin{cases} 1, & \text{if } i \in I_j, \\ 0, & \text{else.} \end{cases}$$

We define

$$\xi_{j,-} := \min_{\xi \in \mathbb{R}} \{\, \xi : \hat{x} + \xi\zeta_j \in C_\alpha(x) \,\} \in \mathbb{R},$$
$$\text{and} \quad \xi_{j,+} := \max_{\xi \in \mathbb{R}} \{\, \xi : \hat{x} + \xi\zeta_j \in C_\alpha(x) \,\} \in \mathbb{R}.$$

Then, we call

$$C^{\text{loc}}_{\alpha,j}(x) := [\hat{x}_{I_j} + \xi_{j,-}\mathbf{1}, \hat{x}_{I_j} + \xi_{j,+}\mathbf{1}] \subset \mathbb{R}^{\#I_j},$$

the I_j-local credible interval (around $\hat{x}$).

Remark 3.3 *To explain the intuition behind Definition 3.2, consider the case where $\mathcal{I} = \{\{1\}, \{2\}, \dots, \{n\}\}$ and suppose that x corresponds to a discretized image. In that case, $\mathbb{R}^n = \mathbb{R}^{n_1 \times n_2}$ is an image space and each coefficient x_i corresponds to a pixel. Then, let $x \in \mathbb{R}^n$ and fix $x_i = \hat{x}_i$ for all $i \neq j$, such that only the j-th pixel may vary. Then, the interval $C^{\text{loc}}_{\alpha,j}(x) \subset \mathbb{R}$ gives all values that x can take at the j-th pixel without leaving the credible region $C_\alpha(x)$.*

Remark 3.4 *The use of different partitions $\mathcal{I}$ has multiple advantages. First, it allows to quantify the uncertainty at different scales. Second, the computation of the local credible intervals requires the solution of $2J$ optimization problems. If $J = n$, this might be computationally very demanding. Hence, one can save significant computation time by using coarser partitions.*

In general, the computation of local credible intervals is very scalable, as it only requires the solution of $2J$ independent one-dimensional optimization problems, which can be done completely in parallel.

However, the locally credible intervals come with one major flaw regarding their interpretation. They only describe the variation of in the credible region at a given superpixel *with the remaining values fixed to the MAP estimate* $\hat{x}$. Thus, the posterior probability that the j-th superpixel lies in the j-th locally credible interval is *not* $1 - \alpha$, and it can actually be much much smaller. The reason for this is that the local credible interval is conditional on all other superpixels being fixed to $\hat{x}$. As an example, if we fix the value of all superpixels around the j-th superpixel to 0, then it is much more improbable that the j-th superpixel will take large values. However, if we allow all superpixels in that region to *vary together* in the credible region $C_\alpha(x)$, then they might take a much larger range of values.

Local credible intervals completely ignore the posterior correlation between the different superpixels. Therefore, the posterior probability that a given superpixel lies in the corresponding local credible interval might actually be arbitrarily small, and it is (at least to me) not clear whether they admit a useful interpretation.

Projected credible intervals

As an anser to the problems of local credible intervals, one can construct credible intervals for each pixel that actually have the right interpretation, namely that the posterior probability of a pixel lying in the given interval is $(1 - \alpha)$. We will call these intervals "projected credible intervals", as they correspond to credible regions of one-dimensional projections of the posterior probability.

Definition 3.5 (Projected credible intervals) Let $p(x)$ be a probability distribution on $\mathbb{R}^n$ and $\alpha > 0$ be given. Then, we call an interval $[a, b] \subset \mathbb{R}$ a projected $(1-\alpha)$-credible interval for the i-th component if

$$\mathbb{P}(x_i \in [a, b]) = \int_{\mathbb{R}^{n-1}} \mathrm{d}x_{-i} \int_a^b \mathrm{d}x_i p(x_1, \dots, x_i, \dots, x_n) \geq 1 - \alpha.$$

In general, the projected credible intervals have to be computed using sampling. However, one can also obtain conservative (i.e. too large) projected credible intervals if one is given a credible region $C_\alpha(x)$. Let

$$\eta_{i,-} \in \operatorname{argmin} \{ x_i : x \in C_\alpha(x) \},$$
$$\eta_{i,+} \in \operatorname{argmin} \{ x_i : x \in C_\alpha(x) \}.$$

Then $[\eta_-, \eta_+]$ is a projected $(1-\alpha)$-credible interval for the i-th component.

From the 3 presented visualizations, the projected credible intervals are the most difficult to compute, as they require the solution of $2n$ n-dimensional optimization problems. At least, these problems are independent and can thus be solved in parallel.

Summary

We summarize the three discussed visualizations in Table 1.

Method	Interpretation	Computation	Advantages	Problems
Minimally/maximally regularized element	The "largest" and "smallest" element in the credible region, where "largest" and "smallest" is defined with respect to the regularization term.	Solution of two n-dimensional optimization problems.	Cheapest to compute, take into account the regularization term.	Do not capture the local variation possible in the credible region
Local credible intervals	Possible deviation from the MAP estimate at given superpixel	Solution of $2n$ independent one-dimensional optimization problems.	Can be defined on different scales, also cheap to compute.	Ignore posterior correlation and can therefore give a misleading representation of the posterior uncertainty (too low).
Projected credible intervals	For each pixel an interval in which the true value of the pixel lies with posterior probability $1-\alpha$.	Solution of $2n$ independent n-dimensional optimization problems.	Clean interpretation.	Expensive to compute.

TABLE 1

From here on, we will focus on the third option, as it is the only one that provides a clean and intuitive interpretation. However, we might keep the other two variants in the back of our head, as we will see that the computation of projected credible intervals can run into problems.

3.2 Ansatz 1: Computing projected credible regions by approximate sampling

Consider the general statistical model

$$\begin{aligned} Y &= F(X_1, X_2) + V, & F &: \mathbb{R}^{n_1} \times \mathbb{R}^{n_2} \to \mathbb{R}^m, \\ X_1 &\sim T_{\mathcal{C}_1}\mathrm{Lap}(\bar{x}_1, \Sigma_1), & \bar{x}_1 &\in \mathbb{R}^{n_1}, P_1 \in \mathbb{R}^{n_1 \times n_1}, \\ X_2 &\sim T_{\mathcal{C}_2}\mathcal{N}(\bar{x}_2, \Sigma_2), & \bar{x}_2 &\in \mathbb{R}^{n_2}, P_2 \in \mathbb{R}^{n_2 \times n_2}, \\ V &\sim \mathcal{N}(0, R), & R &\in \mathbb{R}^{m \times m}, \\ \mathcal{C}_1 &= \{\, x \in \mathbb{R}^{n_1} : A_1 x \geq b_1 \,\}, & A_1 &\in \mathbb{R}^{c_1 \times n_1}, b_1 \in \mathbb{R}^{c_1}, \\ \mathcal{C}_2 &= \{\, x \in \mathbb{R}^{n_2} : A_2 x \geq b_2 \,\}, & A_2 &\in \mathbb{R}^{c_2 \times n_2}, b_2 \in \mathbb{R}^{c_2}. \end{aligned} \tag{3.2}$$

Here, given a set $S \in \mathbb{R}^n$, we defined the truncation operator T_S as follows: Given a probability density function $p : \mathbb{R}^n \to [0, \infty)$, its truncation on the set S is a probability density function $T_S p : S \to [0, \infty)$ given by

$$T_S p(x) := \frac{1}{\int_S p(x)\,\mathrm{d}x} p(x) \mathbb{1}_S(x).$$

Essentially, we are just projecting the probability distribution on the set S and renormalize.

Note that both our pixel-based and our curvelet-based approach are special cases of the model (3.2).

Next, we describe a method to compute approximate projected credible intervals for (3.2).

3.2.1 Nonlinear reparametrization

We start by applying a nonlinear reparametrization. We introduce the map $g_1 : \mathbb{R}^{n_1} \to \mathbb{R}^{n_1}$ which is defined componentwise via

$$g_1(w)_i := \mathrm{sign}(w_i)\,|w_i|^2, \qquad i = 1, \ldots, n_1.$$

This map has the interesting property that it transforms a normal distribution into a Laplace distribution. That is if $W \sim \mathcal{N}(0, \mathbb{I}_{n_1})$, then $g_1(W) \sim \mathrm{Lap}(0, \mathbb{I}_{n_1})$. We can then define a second map $G_1 : \mathbb{R}^{n_1} \to \mathbb{R}^{n_1}$ as

$$G_1(w) := \bar{x}_1 + \Sigma_1^{1/2} g_1(w).$$

Then G_1 maps the normal distribution $\mathcal{N}(0, \mathbb{I}_{n_1})$ to the Laplace distribution $\mathrm{Lap}(\bar{x}_1, \left(\Phi_1 \Phi_1^\top\right)^{-1})$.

We also introduce the map $G_2 : \mathbb{R}^{n_2} \to \mathbb{R}^{n_2}$,

$$G_2(w) := \bar{x}_2 + \Sigma_2^{1/2} w.$$

This map transforms the standard normal distribution $\mathcal{N}(0, \mathbb{I}_{n_2})$ to the normal distribution $\mathcal{N}(\bar{x}_2, P_2)$.

The reason we introduced these maps is that we can now our model to an equivalent model with only Gaussian priors. Define

$$\begin{aligned} & G : \mathbb{R}^{n_1+n_2} \to \mathbb{R}^{n_1+n_2}, \quad G(w) := (G_1(w_1), G_2(w_2)), \qquad w = (w_1, w_2), \\ & H : \mathbb{R}^{n_1+n_2} \to \mathbb{R}^m, \quad H(w) := F(G(w)), \\ \text{and} \quad & \mathcal{D} := G^{-1}(\mathcal{C}_1 \times \mathcal{C}_2) = G_1^{-1}(\mathcal{C}_1) \times G_2^{-1}(\mathcal{C}_2), \end{aligned}$$

Then model (3.2) is equivalent to the model

$$\begin{aligned} Y &= H(W) + V, \\ W &\sim T_{\mathcal{D}}\mathcal{N}(0, \mathbb{I}_n) \\ V &\sim \mathcal{N}(0, R). \end{aligned} \tag{3.3}$$

We have thus transformed our model into a significantly simpler model.

The advantage of these transformations lies in the following fact: If H were linear, the posterior distribution of W given $Y = y$ could be computed explicitly, as the following theorem states.

Theorem 3.6 *Consider the statictical model*

$$\begin{aligned} Y &= HX + V, \\ X &\sim T_{\mathcal{C}}\mathcal{N}(\bar{x}, P), \\ V &\sim \mathcal{N}(0, R), \\ \mathcal{C} &:= \{\, x \in \mathbb{R}^n : \, Ax \geq b \,\}, \end{aligned} \tag{3.4}$$

where $H \in \mathbb{R}^{m\times n}$. *Let*

$$\begin{aligned} x_{\text{post}} &:= \bar{x} + PH^\top \left(HPH^\top + R\right)^{-1}(y - H\bar{x}), \\ \text{and} \quad P_{\text{post}} &:= P - PH^\top \left(HPH^\top + R\right)^{-1} HP. \end{aligned}$$

Then the posterior distribution of X *given* $Y = y$ *is*

$$p_{X|Y}(x|y) = T_{\mathcal{C}}\mathcal{N}(x; x_{\text{post}}, P_{\text{post}}).$$

We cannot apply this result to the statistical model (3.3), because H is nonlinear and the set $\mathcal{D}$ is not given by a linear inequality constraint. In order to apply the theorem, we have to linearize our model. That is, we apply the first-order Taylor approximations

$$H(w) \approx H(\hat{w}) + H'(\hat{w})(w - \hat{w}) \quad \text{and} \quad G(w) \approx G(\hat{w}) + G'(\hat{w})(w - \hat{w}),$$

where $\hat{w} = G^{-1}(\hat{x})$ and $\hat{x}$ is the posteriori mode of X given $Y = y$. With these two approximations, we arrive at the linearized model

$$\begin{aligned} Y &= \tilde{F}(\hat{w}) + \tilde{F}'(\hat{w})(W - \hat{w}) + V, \\ W &\sim T_{\mathcal{D}_{\text{lin}}}\mathcal{N}(0, \mathbb{I}_n), \\ V &\sim \mathcal{N}(0, R), \end{aligned} \tag{3.5}$$

where, using the linearity of G_2, we have

$$\begin{aligned} \hat{w} &= G^{-1}(\hat{x}), \\ \mathcal{D}_{\text{lin}} &= \left\{\, w \in \mathbb{R}^{n_1+n_2} : \, \tilde{A}w \geq \tilde{b} \,\right\}, \\ \tilde{A} &= \begin{bmatrix} A_1 G_1'(\hat{w}_1) & 0 \\ 0 & A_2 G_2'(\hat{w}_2) \end{bmatrix} \in \mathbb{R}^{(c_1+c_2)\times(n_1+n_2)}, \\ \tilde{b} &= \begin{bmatrix} b_1 + A_1 G_1'(\hat{w})\hat{w}_1 - A_1 G_1(\hat{w}_1), \\ b_2 \end{bmatrix} \in \mathbb{R}^{c_1+c_2}. \end{aligned}$$

If we apply Theorem 3.6 to (3.5), we obtain an approximation q of the posterior distribution of W given $Y = y$. It is given by

$$\begin{aligned} q(w|y) &= T_{\mathcal{D}_{\text{lin}}}\mathcal{N}(w; \hat{w}, P_{\text{post}}), \\ \text{where} \quad P_{\text{post}} &:= \left(H'(\hat{w})^\top R^{-1} H'(\hat{w}) + \mathbb{I}\right)^{-1}. \end{aligned} \tag{3.6}$$

3.2.2 Computation of projected credible intervals

Since q is simply a truncated multivariate Gaussian distribution, one can obtain samples from it in a relatively efficient way (at least much more efficient than if we would apply an MCMC algorithm directly to the model (3.2)). These samples can then be transformed into posterior samples of X using the transformation G and be used to compute projected credible intervals for X given $Y = y$.

Algorithm 1 `Projected credible intervals via sampling`

Input: $\hat{x} \in \mathbb{R}^n$, $F(\hat{x}) \in \mathbb{R}^n$, $F'(\hat{x}) \in \mathbb{R}^{m\times n}$, $A_1 \in \mathbb{R}^{c_1\times n}$, $b_1 \in \mathbb{R}^{c_1}$, $A_2 \in \mathbb{R}^{c_2\times n}$, $b_2 \in \mathbb{R}^{c_2}$, the map $G = (G_1, G_2)$, a credibility parameter $\alpha \in (0,1)$ and a sample size J.
Output: The projected credible intervals $[\eta_{1,-}, \eta_{1,+}], \dots, [\eta_{n,-}, \eta_{n,+}] \subset \mathbb{R}$.

1: Set $\hat{w} = G^{-1}(\hat{x})$;
2: Set $P_{\text{post}} = \left(F'(\hat{x})^\top R^{-1} F'(\hat{x}) + \mathbb{I}\right)^{-1}$;
3: Set $\tilde{A}_1 = A_1 G_1'(\hat{w}_1)$;
4: Set $\tilde{b}_1 = b_1 + \tilde{A}_1 \hat{w} - A_1 G_1(\hat{w})$;
5: Generate samples $w_1, \dots, w_J \sim T_{\mathcal{D}_{\text{lin}}}(\hat{w}, P_{\text{post}})$,
6: where $\mathcal{D}_{\text{lin}} = \left\{ (w_1, w_2) \in \mathbb{R}^{n_1+n_2} : \tilde{A}_1 \geq \tilde{b}_1, A_2 \geq b_2 \right\}$;
7: Set $x_j = G(w_j)$ for $j = 1, \dots, J$;
8: **for** $i = 1, ..., n$ **do**
9: Order the coefficients $\tilde{x}_{1i}, \dots, \tilde{x}_{Ji}$ in increasing order and store the result as $\tilde{x} \in \mathbb{R}^J$;
10: Set $i_- = \lfloor \frac{\alpha}{2} J \rfloor$, $i_+ = \lceil (1 - \frac{\alpha}{2}) J \rceil$;
11: Set $\eta_{i,-} = \tilde{x}_{1i_-}$, $\eta_{i,+} = \tilde{x}_{1i_+}$;
12: **end for**
13: return η_-, η_+;

For sampling from the truncated multivariate normal distribution, we used a specialized version of the Gibbs sampler.

3.3 Ansatz 2: Computing projected credible regions by convex optimization

3.3.1 Concentration-based approximation

An alternative estimator that works for linear problems is based on the *concentration of measure* phenomenon. This term describes a collection of mathematical and empirical results which state that the mass of high-dimensional probability distributions tends to be concentrated on lower-dimensional manifolds. Pereyra [2] used this phenomenon to derive an approximation $\tilde{C}_\alpha^2$ of the $(1-\alpha)$-credible region. In the case of a linear statistical model of the form

$$\begin{aligned} Y &= HX + V, \\ X &\sim T_{\mathcal{C}} q, \\ V &\sim \mathcal{N}(0, R), \end{aligned} \tag{3.7}$$

where $H \in \mathbb{R}^{m\times n}$, $\mathcal{C} \subset \mathbb{R}^n$ is a convex set and $q : \mathbb{R}^n \to [0, \infty)$ is a log-concave probability distribution, the estimate is given by

$$\tilde{C}_\alpha^2 = \{\, x \in \mathbb{R}^n : \phi_y(x) \leq \phi_y(\hat{x}) + n(\tau_\alpha + 1) \,\},$$

where ϕ_y is the maximum-a-posteriori cost functional associated to (3.7), given $Y = y$,

$$\phi_y(x) := \left(\frac{1}{2} \|y - Hx\|_2^2 - \log q(x) \right) \mathbb{1}_{\mathcal{C}}(x). \tag{3.8}$$

and $\tau_\alpha := \sqrt{\frac{16 \log(3/\alpha)}{n}}$. It is then shown in [2] that $\tilde{C}_\alpha^2$ is a conservative estimate of the true credible region C_α, i.e. we have

$$C_\alpha \subset \tilde{C}_\alpha^{(2)}.$$

This is a very nice result, because it guarantees that we do not underestimate the uncertainty.

Alas, the result relies on the linearity of H. However, we can use the same strategy as in subsubsection 3.2.1 and simply linearize the model (3.2) at the posterior mode $\hat{x}$. The linearized model is then

$$\begin{aligned} Y &= F(\hat{x}) + F'(\hat{x})(X - \hat{x}) + V, \\ X_1 &\sim T_{\mathcal{C}_1} \text{Lap}(\bar{x}_1, P_1), \\ X_2 &\sim T_{\mathcal{C}_2} \mathcal{N}(\bar{x}_2, P_2), \\ V &\sim \mathcal{N}(0, R). \end{aligned} \tag{3.9}$$

The associated maximum-a-posteriori cost functional is

$$\hat{\phi}_y(x_1, x_2) = \left(\|y - F(\hat{x}) + F'(\hat{x})(x - \hat{x})\|_2^2 + \left\|\Sigma_1^{-1/2}(x_1 - x_1)\right\|_1 + \left\|\Sigma_2^{-1/2}(x_2 - \bar{x}_2)\right\|_2^2 \right) \mathbb{1}_{\mathcal{C}_1}(x_1)\mathbb{1}_{\mathcal{C}_2}(x_2).$$

3.3.2 Projected credible intervals via convex optimization

With the estimator $\hat{C}_\alpha^{(2)}(X|Y = y)$ the computation of projected credible intervals reduces to the solution of $2n$ convex optimization problems: If we want to compute an estimate $\hat{C}_{\alpha,i}^{(2)}(x) = [\eta_{i,-}, \eta_{i,+}]$ of the i-th projected credible interval, we compute the lower and upper bound $\eta_{i,-}$ and $\eta_{i,+}$ as

$$\eta_{i,-} = \min_{x \in \mathbb{R}^n} \left\{ x_i : \hat{\phi}_y(x) \leq \hat{\phi}_y(\hat{x}) + n(\tau_\alpha + 1) \right\},$$
$$\eta_{i,+} = \max_{x \in \mathbb{R}^n} \left\{ x_i : \hat{\phi}_y(x) \leq \hat{\phi}_y(\hat{x}) + n(\tau_\alpha + 1) \right\}.$$

Algorithm 2 `Projected credible intervals via optimization`

Input: $\hat{w} \in \mathbb{R}^n$, $F(\hat{x}) \in \mathbb{R}^n$, $F'(\hat{x}) \in \mathbb{R}^{m \times n}$, $A_1 \in \mathbb{R}^{c_1 \times n}$, $b_1 \in \mathbb{R}^{c_1}$, $A_2 \in \mathbb{R}^{c_2 \times n}$, $b_2 \in \mathbb{R}^{c_2}$, a credibility parameter $\alpha \in (0, 1)$ and a sample size J.
Output: The projected credible intervals $[\eta_{1,-}, \eta_{1,+}], \ldots, [\eta_{n,-}, \eta_{n,+}] \subset \mathbb{R}$.

1: Let $\hat{\phi}(x) := \|y - F(\hat{x}) - F'(\hat{x})(x - \hat{x})\|_2^2 + \left\|\Sigma_1^{-1/2}(x_1 - \bar{x}_1)\right\|_1 + \left\|\Sigma_2^{-1/2}(x_2 - \bar{x}_2)\right\|_2^2$.
2: Set $\tau_\alpha = \sqrt{\frac{16 \log(3/\alpha)}{n}}$;
3: **for** $i = 1, ..., n$ **do**
4: Solve

$$\eta_{i,-} = \min_{x \in \mathbb{R}^n} x_i \quad \text{s.t.} \quad \hat{\phi}(x) \leq \hat{\phi}(\hat{x}) + n(\tau_\alpha + 1), \quad A_1 x_1 \geq b_1, \quad A_2 x_2 \geq b_2.$$

5: Solve

$$\eta_{i,+} = \max_{x \in \mathbb{R}^n} x_i \quad \text{s.t.} \quad \hat{\phi}(x) \leq \hat{\phi}(\hat{x}) + n(\tau_\alpha + 1), \quad A_1 x_1 \geq b_1, \quad A_2 x_2 \geq b_2.$$

6: **end for**
7: return η_-, η_+;

3.4 Results

We have implemented both the sampling- and the optimization-based approaches for computing projected credible intervals. However, the optimization approach was extremely slow, so that we could not obtain results. The sampling approach currently works for the pixel model, but not for the curvelet model. The results for the pixel model with sampling are visualized in Figure 5.

3.5 Discussion

- The uncertainty quantification is challenging. Numerical problems seem to be the main issue.
- The first approach for uncertainty quantification is still sampling-based, even though it samples from a relatively simple distribution. Thus, while it is not super slow, it is also not fast (it is around ten times slower than the MAP estimation).
- Maybe we should consider locally credible intervals (see Section 3.1) as an alternative visualization tool. Their interpretation is not very clear, but they are probably much easier to compute.

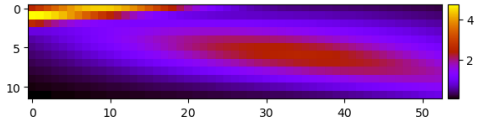

(A) *The true distribution function.*

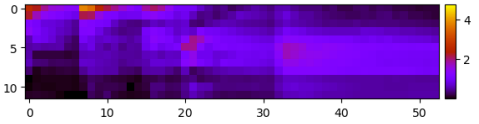

(B) *The MAP estimate.*

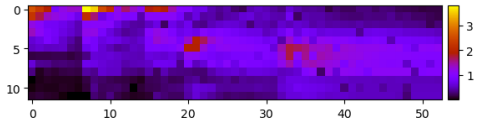

(C) *The lower bound η_- of the projected credible intervals for the distribution function f.*

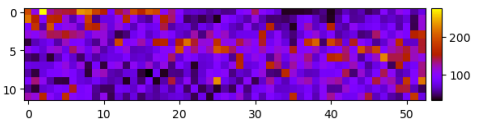

(D) *The upper bound η_+ of the projected credible intervals for the distribution function f.*

FIGURE 5. *Mode-based uncertainty quantification for the pixel-based model: Image (C) shows for each pixel the lower bound of the corresponding projected credible interval, while image (D) shows the corresponding upper bounds.*

References

[1] X. Cai, M. Pereyra, and J. D. McEwen. "Uncertainty quantification for radio interferometric imaging: II. MAP estimation". In: *Monthly Notices of the Royal Astronomical Society* 480.3 (2018), pp. 4170–4182. ISSN: 0035-8711. DOI: 10.1093/mnras/sty2015. URL: https://academic.oup.com/mnras/article-abstract/480/3/4170/5060771?redirectedFrom=fulltext (cited on page 5).

[2] M. Pereyra. "Maximum-a-Posteriori Estimation with Bayesian Confidence Regions". In: *SIAM Journal on Imaging Sciences* 10.1 (2017), pp. 285–302. ISSN: 1936-4954. DOI: 10.1137/16m1071249. URL: https://epubs.siam.org/doi/10.1137/16M1071249 (cited on page 10).